

Magnetization process in $\text{Sm}_{40}\text{Fe}_{60}$ (88 nm)/ $\text{Ni}_{80}\text{Fe}_{20}$ (62 nm) exchange spring filmsD. Chumakov,¹ R. Schäfer,¹ D. Elefant,¹ D. Eckert,¹ L. Schultz,¹ S. S. Yan,² and J. A. Barnard³¹*IFW-Dresden, Helmholtz-Strasse 20, D-01069 Dresden, Germany*²*National High Magnetic Field Laboratory, 1800 E. Paul Dirac Drive, Box 4005, Tallahassee, Florida 32310*³*Department of Materials Science and Engineering, University of Pittsburgh, Pittsburgh, Pennsylvania 15261*

(Received 28 February 2002; revised manuscript received 5 August 2002; published 9 October 2002)

The magnetization reversal in a sputtered $\text{Sm}_{40}\text{Fe}_{60}$ (88 nm)/ $\text{Ni}_{80}\text{Fe}_{20}$ (62 nm) hard/soft bilayer with induced uniaxial anisotropy was investigated by Kerr microscopy and magnetometry. In the reversible regime of the hysteresis loop a twisting of magnetization across the thickness of the soft magnetic film could be derived. The hard layer reverses by the nucleation and growth of regular domains. They are separated from the nonswitched areas by tilted domain walls, the angle of which can be predicted by considering the net magnetic moments of the bilayer system.

DOI: 10.1103/PhysRevB.66.134409

PACS number(s): 75.60.Ch, 75.60.Jk, 75.70.Kw

I. INTRODUCTION

Magnetic bilayers, consisting of two exchange-coupled ferromagnetic films of different magnetic hardness and sufficient thickness above a critical dimension, as shown in Ref. 1, typically display a double step easy axis hysteresis curve [Fig. 1(a)]. After saturation [Fig. 1(b)] and field inversion, the magnetization in the magnetically soft film is continuously twisted across the film thickness [Fig. 1(c)] after exceeding a critical field. At the same time the magnetic moments at the interface are more or less fixed along the previous saturation direction by exchange interaction with the (still rigidly magnetized) hard layer. The twisting is completely reversible, i.e., the soft layer rotates back into alignment with the hard layer if the reverse field is removed—a phenomenon that may be termed “exchange spring” process with reference to exchange spring permanent magnets consisting of nanodispersed hard and soft magnetic coupled phases.² In stronger fields, the soft and hard films are irreversibly remagnetized along the second branch of the hysteresis curve.

Exchange spring films have been investigated in a number of papers.^{1,3–7} Most of them concentrated on the reversal fields of the soft and hard layers and their dependence on the film thickness. Usually hysteresis loops were analyzed to derive information on the magnetization reversal, eventually supported by numerical calculations in which the expected twisting of magnetization in the soft film along the reversible part of the process could be verified.^{3,5,7–9} Microscopic observation was performed in Refs. 6 and 10. Here the average rotation angle in the soft film of an Fe/SmCo bilayer was measured magneto-optically by imaging the fringing fields around etched holes using a magnetic garnet indicator film that was attached to the bilayer in close contact. With this method a field-induced biquadratic coupling effect was found as a consequence of interaction fluctuations due to the partial remagnetization of the fine-grained SmCo layer.⁶ In Ref. 11 domain processes in the buried SmCo film of the same system could be successfully imaged by x-ray microscopy, finding obliquely oriented domain walls that were ob-

viously correlated to structural features in the polycrystalline film.

In general, however, the reversal of the hard film in exchange spring bilayers is treated in a speculative way in the literature. Two possible mechanisms are discussed. The first one is related to the twisted magnetization in the soft film, which may be seen as a Bloch wall parallel to the film plane. With increasing field this wall is increasingly compressed against the hard/soft interface, slowly entering the hard film. It can finally get locally unpinned and quickly sweep across the thickness of the hard film in fields well below the nucleation field of an isolated hard film. This mechanism is for instance suggested in Refs. 3, 8, and 12, stimulated by numerical calculations, and also proposed in Refs. 1 and 4. Alternatively, the hard film could as well be irreversibly switched by the nucleation and growth of regular domains with walls that propagate laterally along the film. This reversal mechanism was suggested in Ref. 5, derived from minor magnetization loops. In any case, a direct observation of domain processes is expected to provide important information on the real mechanism in each sample system.

In this paper the magnetization reversal in a sputtered $\text{Sm}_{40}\text{Fe}_{60}$ (88 nm)/ $\text{Ni}_{80}\text{Fe}_{20}$ (62 nm) bilayer film was there-

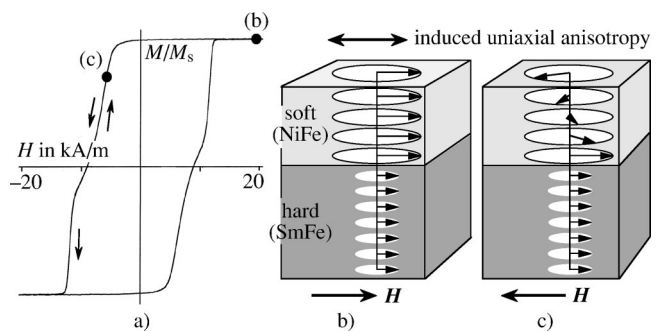


FIG. 1. (a) Easy axis magnetization curve of a $\text{Sm}_{40}\text{Fe}_{60}$ (88 nm)/ $\text{Ni}_{80}\text{Fe}_{20}$ (62 nm) bilayer film with an induced uniaxial anisotropy. Sketches (b) and (c) schematically show the expected twisting of magnetization in the soft film along the reversible branch of the hysteresis curve.

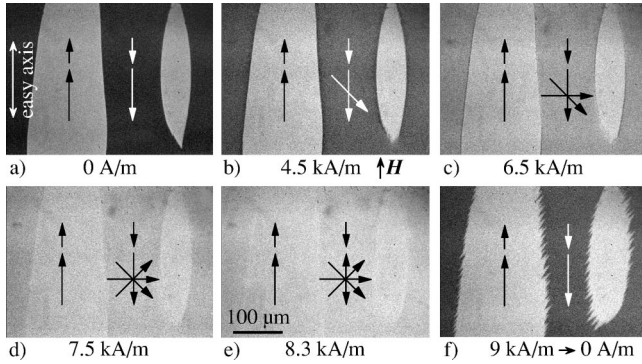


FIG. 2. Domain observation on the NiFe side of the NiFe/SmFe bilayer. In an increasing field the NiFe magnetization is reversibly twisted or rotated [(a)–(e)]. Beyond about 9 kA/m the domain walls are irreversibly shifted (f).

fore studied by Kerr microscopy. This is one sample out of a series of SmFe/NiFe bilayers that were thoroughly investigated in Ref. 1. Both the amorphous SmFe film and the nanocrystalline NiFe (permalloy) film have an induced uniaxial anisotropy along the same axis with anisotropy fields of 300 kA/m and some kA/m, respectively, as estimated from the saturation fields of hard axis hysteresis loops of corresponding single films. This justifies the assumption of an approximately rigid magnetization in the SmFe film in the relevant applied field range of about 10 kA/m. The saturation polarizations of SmFe and NiFe are 0.36 and 1.08 T, respectively, which results in different magnetic moment fractions of 0.68 for NiFe and 0.32 for SmFe (by considering the film thicknesses of 88 and 62 nm, respectively). In some figures the magnetization of the two films is therefore indicated by vectors of different length.

II. EXPERIMENT

The $\text{Sm}_{40}\text{Fe}_{60}$ (88 nm)/ $\text{Ni}_{80}\text{Fe}_{20}$ (62 nm) bilayer was prepared by dc magnetron sputtering at room temperature on a glass substrate that allows domain observation from both sides. The deposition rates were 0.15 nm/s and 0.16 nm/ms for NiFe and SmFe, respectively. An in-plane uniaxial anisotropy was induced with the easy axis along the direction of a permanent magnetic field of 6 kA/m being present during deposition. The bilayer was protected by a 5-nm Si_3N_4 layer that was rf sputter deposited *in situ*. The structure of the films was characterized by routine θ - 2θ x-ray diffraction. The nanocrystallinity of the NiFe film was indicated by a wide peak of fcc(111)-NiFe around 43.7° , and a very broad peak located between 27° and 37° indicated the amorphous state of the SmFe film.

The magnetization loops were measured in an alternating gradient magnetometer (AGM) and by superconducting quantum interference device (SQUID) magnetometry. Domain observation was performed in a digitally enhanced Kerr microscope applying the longitudinal Kerr effect with the axis of sensitivity along the magnetically preferred axis.

III. DOMAIN OBSERVATION

The spring process is demonstrated by domain observation on the NiFe side in Fig. 2. By demagnetization in an

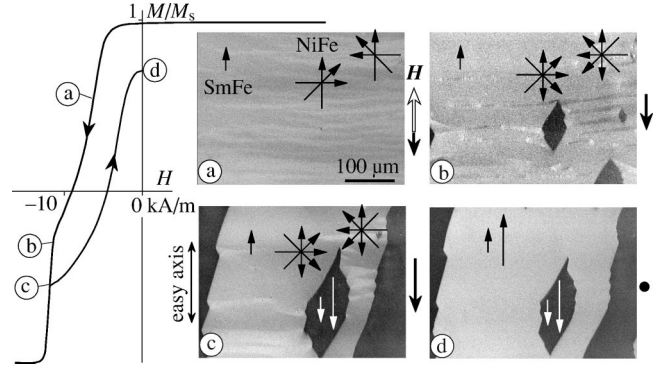


FIG. 3. Easy axis magnetization process along the hysteresis curve, observed from the NiFe side. The reversible branch is characterized by a striplike modulation of magnetization (a), the irreversible branch by the nucleation and growth of regular domains [(b) and (c)]. The field direction is marked by arrows on the side of each picture. The open arrow at (a) marks the previous saturation direction.

alternating magnetic field along the easy axis it is possible to obtain a 180° domain state [Fig. 2(a)], in which the SmFe and NiFe films are magnetized parallel. In a magnetic field along the direction of the white domains, the magnetization in the black NiFe domains is rotated (presumably twisted) so that the black domains continuously approach the color of the white domains with increasing field strength [Figs. 2(b)–2(e)]. Up to about 9 kA/m this rotational process is reversible without wall motion, i.e., the SmFe domains are not affected. In fields stronger than 9 kA/m the domain walls are shifted and zigzag folded as shown in the remanence picture of Fig. 2(f).

The complete demagnetization process, again observed from the NiFe side, is shown in Fig. 3. Here the external field was precisely aligned along the preferred axis. After saturation and field inversion, the magnetization in the NiFe film becomes simultaneously twisted clockwise and counterclockwise on a local scale during demagnetization. The two phases of opposite chirality appear in a characteristic contrast texture orthogonal to the field direction [Fig. 3(a)] in a similar way as magnetization ripple in polycrystalline single films after decreasing a hard axis field.¹³ The simultaneous presence of both chiralities can be seen as a reaction of the permalloy film to a statistical perturbation by the crystal anisotropy of the individual grains (like in the ripple phenomenon¹⁴). The orthogonal texture is caused by the stray field energy: a modulation of magnetization around a mean direction along the field direction (which in our case is caused by both chiralities) is energetically more favorable if both phases are separated by “walls” that are running orthogonal to the field direction. In Ref. 10 a similar conclusion on the magnetization process in the soft magnetic layer was derived from fringing field imaging around holes using the mentioned magneto-optic indicator technique on CoSm/Fe bilayers. If the field would be reduced from any point on the reversible branch of the magnetization curve, the stripes would reversibly disappear due to the exchange interaction with the (still rigidly magnetized and saturated) hard layer. At the onset of the irreversible branch, the hard

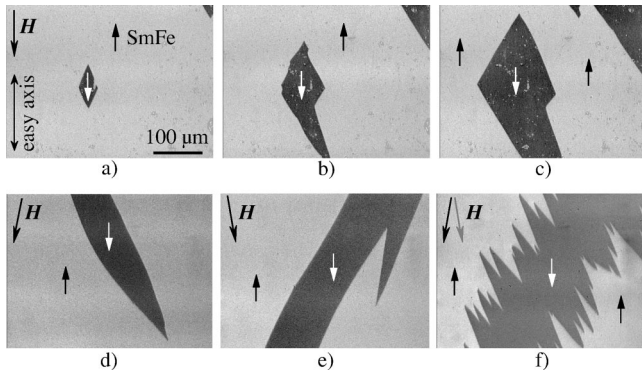


FIG. 4. (a)–(c) Magnetization process in an easy axis field along the irreversible branch of the magnetization curve, observed from the SmFe side. In (d) and (e) the field was misaligned by $\pm 5^\circ$ away from the easy axis. Image (f) is related to (e) as explained in the text. The arrows mark the magnetization direction in the SmFe film.

and soft layer are irreversibly switched by the nucleation [Fig. 3(b)] and growth (c) of black domains. In these domains, which are separated from the twisted matrix by zigzag walls, both films are magnetized parallel along the field direction. If the field is turned off somewhere on the irreversible branch, the black domains almost stay unaffected, whereas the twisted areas in the NiFe film return to the previous direction, thus forming a 180° domain pattern with a parallel magnetization in both films (d).

In Fig. 4 the same process was observed on the SmFe side. As the twisting cannot be seen from this side, only the nucleation and growth along the irreversible branch are displayed [Figs. 4(a)–4(c)]. The zigzag character of the domain walls is well pronounced in these images. The occurrence of the zigzags requires the simultaneous presence of both chiralities in the NiFe film as will be discussed in Sec. IV. This is only possible if the magnetic field is exactly aligned along the preferred axis within one degree. The wall angles can be isolated by slightly misaligning the field, thus uniquely selecting one of the two possible chiralities: rotating the field direction clockwise results in the nucleation of counterclockwise domain walls [Fig. 4(d)] and vice versa [Fig. 4(e)]—note that the zigzag in Fig. 4(e) is not related to the chirality induced zigzag. It is rather caused by wall pinning]. If, starting from the latter domain state, the field is rotated clockwise again [Fig. 4(f)] the previous overall wall

orientation of Fig. 4(e) is maintained, but the walls become folded along the axis of Fig. 4(d).

A domain state similar to that in Fig. 4(e) is shown in Fig. 5. After switching off the magnetic field, the domains were imaged from the NiFe and SmFe side separately by turning around the sample. Both images show identical domains, proving that the reversed domains along the irreversible branch of the hysteresis curve extend across both, soft and hard layer.

IV. DISCUSSION

The domain-wall angles during irreversible switching can be explained in terms of net local magnetic moments. As indicated in Fig. 6(a), the moment fractions of 0.68 for NiFe and 0.32 for SmFe add up to a total (normalized) moment of $+1$ at positive saturation. The magnetic field shall be aligned precisely along the easy axis that is identical with the x axis in the coordinate system of Fig. 6(b).

After field inversion [Fig. 6(b)], the magnetization in the NiFe film is twisted clockwise or counterclockwise, whereas the SmFe film is assumed to remain magnetized positively as long as we stay on the reversible branch of the hysteresis loop. This is schematically indicated in the left part of Fig. 6(b). The SmFe and NiFe moments add up to a net magnetization vector \mathbf{m}_1 , the direction of which depends on the chirality in the NiFe film. On entering the irreversible branch, domain nuclei are formed in which the SmFe magnetization is flipped by 180° , forcing the NiFe magnetization along the same direction by exchange coupling. The nucleus is represented by a magnetization vector \mathbf{m}_2 in the right part of Fig. 6(b). The three domain phases are separated by domain walls that have to obey the condition $(\mathbf{m}_1 - \mathbf{m}_2) \cdot \mathbf{n} = 0$ to be globally free of net magnetic charge (note that the walls themselves can nevertheless be locally charged in a dipolar way if they are of Néel character). The wall normal $\mathbf{n} = (\cos \varphi, \sin \varphi)$ is defined in Fig. 6(b).

To calculate the wall angles of the domain nucleus, the two vector components of \mathbf{m}_1 have to be determined. The x component (i.e., the component along the field direction) can directly be taken from the hysteresis loop: it is the magnetization value at the onset point of irreversible switching [see Fig. 6(c)]. This point is obtained by measuring the minor loops at successively increasing reversal fields. At the onset of irreversible switching, the minor loops become irreversible. The problem is, that the onset point is ill defined for our sample as the irreversible switching is strongly time dependent. This is demonstrated in Fig. 6(c), where the magnetization curves measured at three different speeds are plotted. The curves at 2000 and 200 A/m per sec were obtained in the AGM magnetometer, the 2-A/m/sec curve was measured in a SQUID magnetometer. The onset point is shifted towards higher fields and larger negative magnetization with increasing measurement speed. This means that thermal activation plays an important role in the nucleation and unpinning of reversed domains. The time dependence can also be observed in the Kerr microscope: once an irreversible nucleus is formed, the domain walls tend to creep. To determine the magnetization components at domain nucleation, we there-

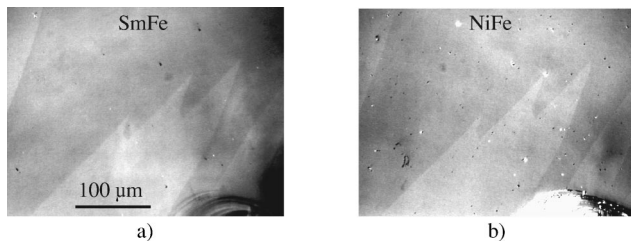


FIG. 5. Identical domains on the SmFe (a) and NiFe side (b), imaged separately by turning around the sample. The second image was mirrored around the vertical axis to allow a direct comparison of the pictures. Unprocessed raw images are shown in each case.

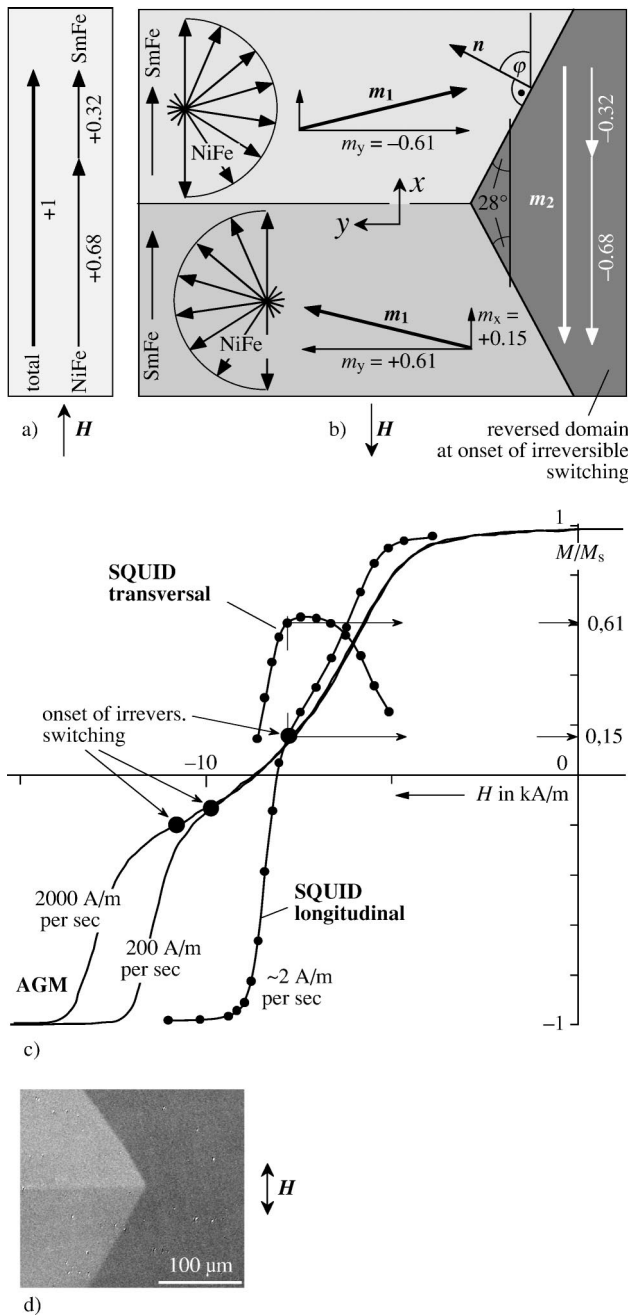


FIG. 6. Magnetization model for the explanation of the domain wall angles. In (a) the bilayer is saturated in a positive field. In (b) a reversed domain is formed on the right, which is separated by tilted walls from the twisted zones on the left. The magnetization vector \mathbf{m}_1 was determined from the magnetization curves in (c), where the longitudinal and transverse components are plotted as measured by AGM and SQUID magnetometry. Kerr image (d) verifies the coexistence of three domain phases as assumed in (b).

fore have chosen the onset point of irreversible switching derived from the low-speed SQUID curve. This onset field is in the same range as the nucleation field determined by microscopy at a slowly varying field. Another interesting observation is the delay in the reversible branch of the SQUID magnetization curve as compared to the AGM curves. This might be related to the AGM technique, in which an alter-

nating field gradient (of about 100 A/m/mm) is superimposed to the stepwise changing dc field. The alternating field could influence the magnetization process by causing domain states that are closer to equilibrium.

For the SQUID curve also the transversal component (y component) of \mathbf{m}_1 was measured [Fig. 6(c)]. To avoid a cancellation of the transverse moment, it was necessary to misalign the field by a few degrees from the easy axis, so that just one chirality in the NiFe film is selected. Around the onset of irreversible switching, at which m_{1x} is +0.15, the m_{1y} component amounts to about +0.61. With $\mathbf{m}_1 = (+0.15, +0.61)$, $\mathbf{m}_2 = (-1, 0)$, and $\mathbf{n} = (\cos \varphi, \sin \varphi)$ we get $\varphi = -62^\circ$ for the wall normal direction under the condition of net-charge freedom. By symmetry, this results in the two possible wall orientations of $\pm 28^\circ$ as sketched in Fig. 6(b). Experimentally an angle of about $\pm 23^\circ$ is measured at the nucleus of Fig. 4(a).

The observations in Figs. 6(d) and 4(f) support our model. In Fig. 6(d), observed from the NiFe side, the three domain phases are visible. However, the picture is not taken at nucleation, but after the irreversible switching was already in progress. The field was then stopped and somewhat reduced to avoid creeping. A wall angle of about $\pm 30^\circ$ is measured in this picture. Also the zigzag walls in Fig. 4(f) can now be explained. Previous to the domain state shown there, the state of Fig. 4(e) was obtained during irreversible switching in a field slightly misaligned by about $+5^\circ$ relative to the preferred axis. The field amplitude was then reduced to zero, rotated to -5° and increased again. Now the chirality in the NiFe film is opposite to the previous one, so that a wall orientation like in Fig. 4(d) would be favored. The walls of Fig. 4(e) tend to approach this orientation by zigzag folding in Fig. 4(f). Similar arguments apply to the zigzag walls in Fig. 2(f). By demagnetizing the sample in a field close to the easy axis, it was possible to create the 180° domain state of Fig. 2(a). For increasing fields [Figs. 2(b)–2(e)] the black domains get increasingly twisted. This creates a transverse magnetization component in these domains so that the initial wall orientation becomes unfavorable. Nevertheless, the domain walls remain straight as long as we stay on the reversible branch of the hysteresis curve. The gain in energy by reorienting the walls is obviously not strong enough to overcome coercivity forces. Only in stronger fields that initiate irreversible wall motion [Fig. 2(f)] do the walls approach their required equilibrium orientation by zigzag folding, keeping their overall orientation at the same time. The zigzag state is obviously preserved after switching off the field, again due to coercivity effects. Further information on the zigzag folding of domain walls can be found in Ref. 13.

Although our domain observations show the growth of regular domains during irreversible switching, they do not answer the question of the nucleation mechanism. Note that in single SmFe films in the same thickness range nucleation fields of more than 40 kA/m are observed,¹ which is at least four times as large as found for the bilayer. A conceivable interpretation of the reduced nucleation field of the bilayer could be fluctuations in the interface coupling: At locations with stronger interface coupling a stronger twisting of the soft layer magnetization might occur with an in-plane Bloch

wall that is successively compressed towards the interface, eventually entering the hard film and thus forming a nucleus. This nucleus then grows laterally by the motion of regular domain walls.

An interesting feature, derived from the SQUID curves, has to be noted. The SQUID curve in Fig. 6(c) reveals a maximum transverse moment of about 0.63, which is 93% of the total moment of the NiFe film. For comparison, a transverse moment of only 73% can be derived from the SQUID curves of a $\text{SmCo}(20\text{ nm})/\text{Fe}(20\text{ nm})$ bilayer investigated in Ref. 3. Two effects can possibly contribute to the surprisingly large transverse moment measured in our SmFe/NiFe system: (i) The twisting in the permalloy film might not be as pronounced as in the SmCo/Fe system where the films are even thinner than in our case. A more homogeneous rotation of magnetization would then have to be assumed and consequently a reduced exchange coupling across the hard/soft interface as compared to the exchange stiffness in the NiFe film, which allows a rapid rotation of spins at the interface and a low degree of twisting across the soft film thickness. (ii) There might also be a considerable twisting in the SmFe film. Micromagnetic simulations would be necessary to decide on the contributions of both effects. However, they would require the knowledge of the strength of exchange coupling across the hard/soft interface that is unknown.

V. SUMMARY

The magnetization reversal in a sputtered $\text{Sm}_{40}\text{Fe}_{60}$ (88 nm)/ $\text{Ni}_{80}\text{Fe}_{20}$ (62 nm) bilayer film with induced

uniaxial anisotropy was investigated by Kerr microscopy. The low-anisotropy NiFe film is exchange coupled to the high-anisotropy amorphous SmFe film, leading to a double step easy axis hysteresis curve as typical for an exchange spring film system. Along the reversible part of the curve the magnetization in the soft film is continuously rotated in a stripelike way, indicating clockwise and counterclockwise rotation. The simultaneous measurement of longitudinal and transverse magnetization components indicates a surprisingly high transverse magnetic moment in our bilayer system. Micromagnetic calculations, which correctly consider the (unknown) coupling across the interface, would be necessary to quantitatively derive the spin structure.

Along the irreversible curve, hard and soft layers are switched by the nucleation and growth of regular domains rather than by a domain wall that propagates along the film thickness direction. The domains are separated from the rotated matrix by characteristically tilted domain walls. The wall angles can be explained in terms of the local net magnetization under the constraint of charge freedom.

ACKNOWLEDGMENTS

The authors want to thank Ulrich Rössler and Alex Bogdanov for helpful discussions. Thanks also to Jeffrey McCord for critically reading the manuscript. S.S.Y. and J.B. wish to thank DARPA, No. DAAD 19-01-1-0546, for support.

¹S.-S. Yan, J. A. Barnard, F.-T. Xu, J. L. Weston, and G. Zangari, *Phys. Rev. B* **64**, 184403 (2001).

²E. F. Kneller and R. Hawig, *IEEE Trans. Magn.* **27**, 3588 (1991).

³E. E. Fullerton, J. S. Jiang, M. Grimsditch, C. H. Sowers, and S. D. Bader, *Phys. Rev. B* **58**, 12 193 (1998).

⁴S. Mangin, G. Marchal, C. Bellouard, W. Wernsdorfer, and B. Barbara, *Phys. Rev. B* **58**, 2748 (1998).

⁵T. Nagahama, K. Mibu, and T. Shinjo, *J. Phys. D* **31**, 43 (1998).

⁶V. K. Vlasko-Vlasov, Z. Welp, J. S. Jiang, D. J. Miller, G. W. Crabtree, and S. D. Bader, *Phys. Rev. Lett.* **86**, 4386 (2001).

⁷M. Grimsditch, R. Camley, E. E. Fullerton, S. Jiang, S. D. Bader, and C. H. Sowers, *J. Appl. Phys.* **85**, 5901 (1999).

⁸E. E. Fullerton, J. S. Jiang, and S. D. Bader, *J. Magn. Magn. Mater.* **200**, 392 (1999).

⁹K. Mibu, T. Nagahama, and T. Shinjo, *J. Magn. Magn. Mater.* **163**, 75 (1996).

¹⁰R. D. Shull, A. J. Shapiro, V. S. Gornakov, V. I. Nikitenko, J. S. Jiang, H. Kaper, G. Leaf, and S. D. Bader, *IEEE Trans. Magn.* **37**, 2576 (2001).

¹¹J. Pollmann, G. Srajer, D. Haskel, J. C. Lang, J. Maser, J. S. Jiang, and S. D. Bader, *J. Appl. Phys.* **89**, 7165 (2001).

¹²S. Wehner, J. C. Toussaint, and J. Voiron, *Phys. Rev. B* **55**, 11 576 (1997).

¹³A. Hubert and R. Schäfer, *Magnetic Domains: The Analysis of Magnetic Microstructures* (Springer-Verlag, Berlin, 1998).

¹⁴H. Hoffmann, *IEEE Trans. Magn.* **4**, 32 (1968).